

Observing Ultra-High Energy Cosmic Rays with Smartphones

Daniel Whiteson,^{1,2} Michael Mulhearn,³ Chase Shimmin,² Kyle Cranmer,⁴ Kyle Brodie,² and Dustin Burns³

¹ Corresponding author: daniel@uci.edu

²Department of Physics and Astronomy, University of California, Irvine, CA 92697

³Department of Physics, University of California, Davis, CA

⁴Department of Physics, New York University, New York, NY

We propose a novel approach for observing cosmic rays at ultra-high energy ($> 10^{18}$ eV) by repurposing the existing network of smartphones as a ground detector array. Extensive air showers generated by cosmic rays produce muons and high-energy photons, which can be detected by the CMOS sensors of smartphone cameras. The small size and low efficiency of each sensor is compensated by the large number of active phones. We show that if user adoption targets are met, such a network will have significant observing power at the highest energies.

Introduction

The source of ultra-high energy cosmic rays (UHECR), those with energy above 10^{18} eV, remains a puzzle even many decades after their discovery, as does the mechanism behind their acceleration. Their high energy leaves them less susceptible to bending by magnetic fields between their source and the Earth, making them excellent probes of the cosmic accelerators which produce them [1, 2]. But the mechanism and location of this enormous acceleration is still not understood, despite many theoretical conjectures [3–6].

When incident on the Earth’s atmosphere, UHECRs produce extensive air showers, which can be detected via the particle flux on the ground, the fluorescence in the air, or the radio and acoustic signatures. A series of dedicated detectors [7–9] have detected cosmic rays at successively higher energies, culminating in observation up to $3 \cdot 10^{20}$ eV. The flux of particles drops precipitously above 10^{18} GeV, due to the suppression via interaction with the cosmic microwave background [10, 11], making observation of these particles challenging.

To accumulate a sufficient number of observed showers requires either a very long run or a very large area. Constructing and maintaining a new detector array with a large effective area presents significant obstacles. Current arrays with large, highly-efficient devices (Auger [12], Telescope Array [13], AGASA [14]) cannot grow dramatically larger without becoming much more expensive. Distributed detector arrays with small, cheaper devices (*e.g.* ERGO [15]) have the potential to grow very large, but have not achieved the size and density required to probe air showers, potentially due to the organizational obstacles of production, distribution and maintenance of their custom-built devices.

It has been previously shown that smartphones can detect ionizing radiation [16–18]. In this paper, we demonstrate that a dense network of such devices has power sufficient to detect air showers from the highest energy cosmic rays. We measure the particle-detection efficiency

of several popular smartphone models, which is necessary for the reconstruction of the energy and direction of the particle initiating the shower. With sufficient user adoption, such a distributed network of devices can observe UHECRs at rates comparable or exceeding conventional cosmic ray observatories. Finally, we describe the operating principles, technical design and expected sensitivity of the CRAYFIS (Cosmic RAYS Found In Smartphones) detector array. Preliminary applications for Android and iOS platforms are available for testing [19].

Detection

Air showers induced by cosmic rays contain an enormous number of particles. Figure 1 shows the energy spectrum, and spatial distribution at sea level of photons, electrons, and muons in showers as simulated by the CORSIKA [20] program with the QGS-II [21] model of hadronic interactions.

We focus our attention on photons, which have high densities in the shower, and muons, which have excellent penetrating power and high detection efficiency. Electrons are also numerous and have high efficiency, but may be blocked by buildings, phone cases or camera lenses. Heavier hadronic particles are much less common.

The sensitive element in a smartphone is the camera, a CMOS device in which silicon photodiode pixels produce electron-hole pairs when struck by visible photons. While these devices are designed to have reasonable quantum efficiency for visible light, the same principle allows the sensor to detect higher-energy photons [16] as well as minimally-ionizing particles such as muons [22, 23].

Our own GEANT-based simulation [24] of muons, protons, electrons and photons incident on a simple block of Silicon confirms that there is significant interaction and energy deposition for incident particles in the energy range expected in an air shower. The modeling of the microphysical processes involved have been validated extensively in the context of silicon-strip detectors for

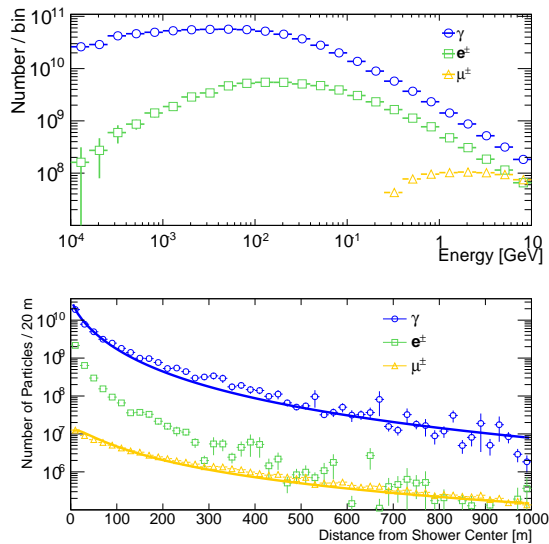


FIG. 1: Energy spectrum (a) and distance from shower axis (b) of photons, electrons, and muons at ground level for simulated air showers initiated by protons with energy $10^{19} - 10^{20}$ eV. Also shown (b) is a parametric fit to Eq 1.

particle physics experiments, though the specifics of the doping and electric-field configuration needed for readout differ substantially between collider silicon-based detectors and CMOS devices and have not been included in this initial study.

An application running on the smartphone has access to an array of *pixel response* values, commonly with eight-bit precision. Though many stages of processing occur between the direct measure of the deposited energy by the CMOS sensor and the delivery of pixel response values, we assume that the former is a reasonable proxy for the latter.

Software

With the camera as the detector element, the phone processor runs an application which functions as the trigger and data acquisition system. To obtain the largest possible integrated exposure time, the first-level trigger captures video frames at 15-30 Hz, depending on the frame-processing speed of the device. Frames which contain any above-threshold pixels are stored and passed to the second stage which examines the stored frames, saving only the pixels above a second, lower threshold. All qualifying pixels, typically a few per frame, are stored as a sparse array in a buffer on the phone, along with their arrival time and the geolocation of the phone. When a wi-fi connection is available, the collected pixels are uploaded to a central server for offline shower reconstruction; most events are between 50 – 200 bytes of data. The acquired event rate may be tuned by setting the

thresholds to eliminate spurious background events; typical rates are around 0.2 Hz.

The application is designed to run when the phone is not in active use and a power source is available. No additional light shielding of the camera, such as tape, is required, other than placing the phone face-up (camera-down) on a table. In a few devices tested, performance at night-time without shielding was equivalent to tests done with shielding; this performance may vary with model type. Real performance will vary according to the device camera geometry as well as the ambient conditions; per-device calibration will be important in establishing backgrounds levels. In this way, no active participation is required once the application is installed and its operation should be fairly unobtrusive, which is critical to achieving wide participation in the smartphone community. To address user privacy concerns, no frames will be stored or uploaded if the average pixel response value over the frame exceeds a threshold, such that full images cannot be reconstructed offline.

Offline, we perform hot-pixel removal. Individual pixels that fire at a rate much higher than the average are removed; these are caused either by light leakage, typically near the edge of the frame, or by poorly-performing or noisy pixels.

Photon Reconstruction and Efficiency

Detection of particles in smartphones has been performed previously [16], but application of such measurements to the observation of extensive air showers from UHECRs has not yet been explored. A critical step is understanding the product of active area and the efficiency $A\epsilon$ of each device for the particles species in an air shower. The number of events N_{cand} that pass the trigger threshold determines the efficiency $\epsilon = N_{\text{cand}}/N_{\text{incident}}$ of the device. Measurements of the efficiency are presented below, and details of A are typically available from manufacturers.

The response of several popular phone models to photons was measured in the lab using gamma rays from the radioactive decays of Ra^{226} ($E_\gamma = 30 - 600$ keV), Co^{60} ($E_\gamma = 1.2 - 1.3$ MeV) and Cs^{137} ($E_\gamma \leq 700$ keV). As a representative example, the measured pixel response of a Samsung Galaxy S3 is shown in Fig. 2; similar spectra are seen in other Android models as well as iPhones. In the presence of radioactive sources, the camera detects pixels with a large charge deposition at a rate that is proportional to the activity of our sources. When no source is nearby, the distribution of pixel response values presents a steeply falling distribution, with a long tail that we attribute to cosmic ray muons (see discussion below). To confirm the sensitivity of the phones to photons, we periodically place a radioactive source near a phone and remove it; Fig. 3 shows that the number of pixels with a

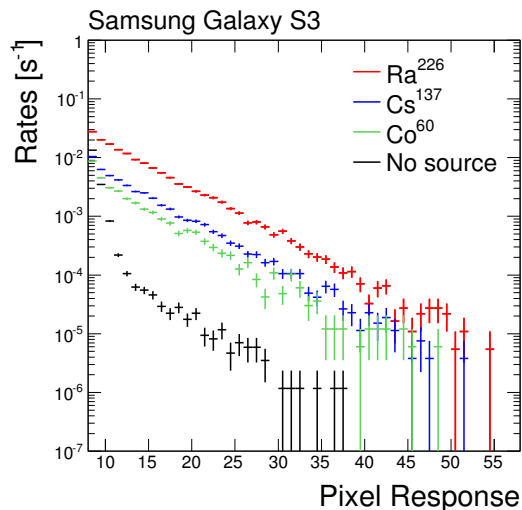


FIG. 2: Distribution of observed pixel response values in a Samsung Galaxy S3 phone when exposed to sources which emit photons between 30-1200 keV, and without any source. The differences in rates are due to the different activity of the sources. The data with no source shows a falling noise distribution and a tail attributed to cosmic muons. Other phone models show qualitatively similar behavior.

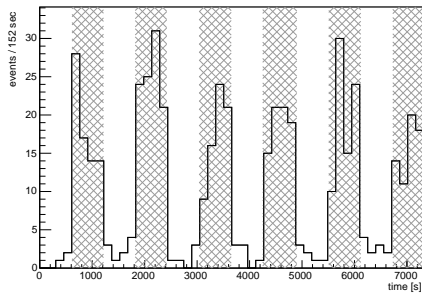


FIG. 3: Number of pixels with value above trigger threshold versus time in a Samsung Galaxy S3 phone. In the periods indicated by hatching, a ^{226}Ra source has been placed near the phone.

value above a trigger threshold is highly correlated with the presence of a radioactive source. In addition to leaving isolated pixels with large pixel response values, some high energy photons leave several bright pixels in clusters or tracks; see Fig. 4. These can be attributed to compton-scattered and pair-produced electrons.

For a radioactive source with activity R a distance d from the sensor, we can measure $A\epsilon$ by counting the number of events observed N_{obs} over a period Δt :

$$A\epsilon = 4\pi d^2 \frac{N_{\text{obs}}}{R\Delta t}.$$

The activity of each radioactive source was determined using a high-precision photon counter at the UC Irvine

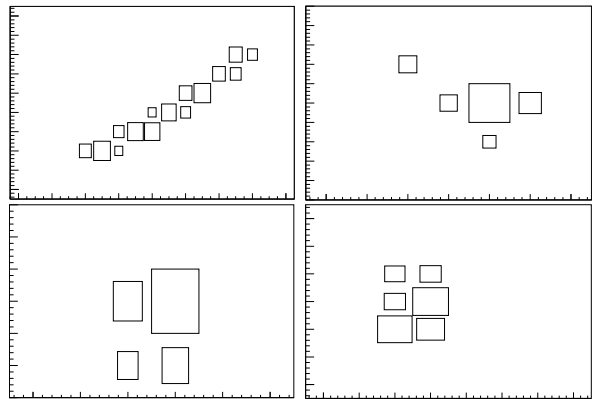


FIG. 4: Activated pixels above threshold in a Samsung Galaxy SIII phone, during exposure to ^{60}Co . Box size is proportional to pixel response values

test reactor. The distance from the camera to the source was kept constant using a wax assembly, allowing us to measure $A\epsilon$ to within a few percent. We found only minor variation in $A\epsilon$ for the different photon sources listed above. Between the different phone models tested, we measured a range of $A\epsilon$ of $2.5 \times 10^{-9} - 2.5 \times 10^{-8} \text{ m}^2$, with consistent values of $A\epsilon$ between phones of the same model. We therefore consider a conservative range of average photon sensitivity of $A\epsilon = (1 - 5) \times 10^{-9} \text{ m}^2$ for projections. Note that improved background suppression at the trigger level could yield increased photon candidate efficiency.

Muon Reconstruction and Efficiency

Muon efficiencies for each device are calculated by comparing the rate of candidate muons to the expected rate from cosmic ray muons. In surface experiments, at least 5 cm of lead shielding was used to suppress contributions from ambient radioactivity. Runs at higher altitude during commercial airline flights display an increase in observed charged particle candidates, consistent with expectation. However, the uncertainty in both the actual local muon flux and the fraction of candidate muons which are due to other sources (such as electronic noise or background radioactivity) lead to large uncertainty on the muon efficiency. For this reason we consider two benchmark muon $A\epsilon$ scenarios which reflect the uncertainty in the muon efficiency and variation in sensor sizes. Composite images from phones exposed to a muon beam at CERN in Geneva, Switzerland are shown in Fig. 5. The beam was incident on the side of the phone, and the image has clear muon tracks from that direction; the nearly unbroken nature of these tracks implies a fairly high efficiency. Studies using a muon telescope to tag muon candidates and directly measure the per-pixel efficiency to muons are currently underway.

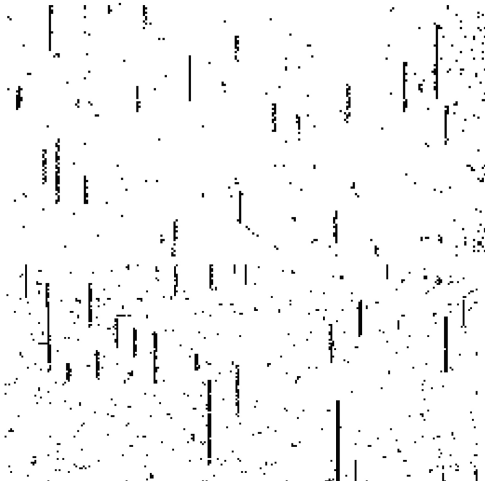


FIG. 5: Composite image of activated pixels in data collected from phones exposed to a muon beam. The phones were arranged such that the muon beam was incident on the side of the sensor, giving visible tracks where muons pass through several pixels.

Shower Reconstruction

In the presence of an air shower, the local density of particles can be written as a vector $\rho(x, y)$, where each component refers to a particular species of particle (muon or photon). A phone, with active detector element area A , and particle species identification efficiency vector $\epsilon = (\epsilon_\mu, \epsilon_\gamma)$, will reconstruct a mean number of candidates $\lambda = \eta + A\epsilon \cdot \rho(x, y)$, where η is the expected number of uncorrelated hits from background sources due to electronic noise, uncorrelated muons and ambient radioactivity in a coincidence window.

The probability that a phone will register no candidates is then given by the Poisson distribution

$$P_0(x, y) = e^{-A\epsilon \cdot \rho(x, y) - \eta},$$

and the probability that the phone will register one or more candidates is

$$P_1(x, y) = 1 - e^{-A\epsilon \cdot \rho(x, y) - \eta}.$$

If the quantity $A\epsilon$ is known for each phone and particle species type, measuring the distribution of phones with and without candidates constrains the local shower density $\rho_i(x, y)$, of each particle species i . The density is directly proportional to the incident particle energy with a distribution in x and y sensitive to the incident particle direction. We use a parameterized model for ρ [25]

$$\rho(N_i, r, s) = \frac{N_i}{2\pi r_M^2} \left(\frac{r}{r_M}\right)^{(s-2)} \left(1 + \frac{r}{r_M}\right)^{(s-4.5)} \times \left(\frac{\Gamma(4.5-s)}{\Gamma(s)\Gamma(4.5-2s)}\right) [\text{m}^{-2}] \quad (1)$$

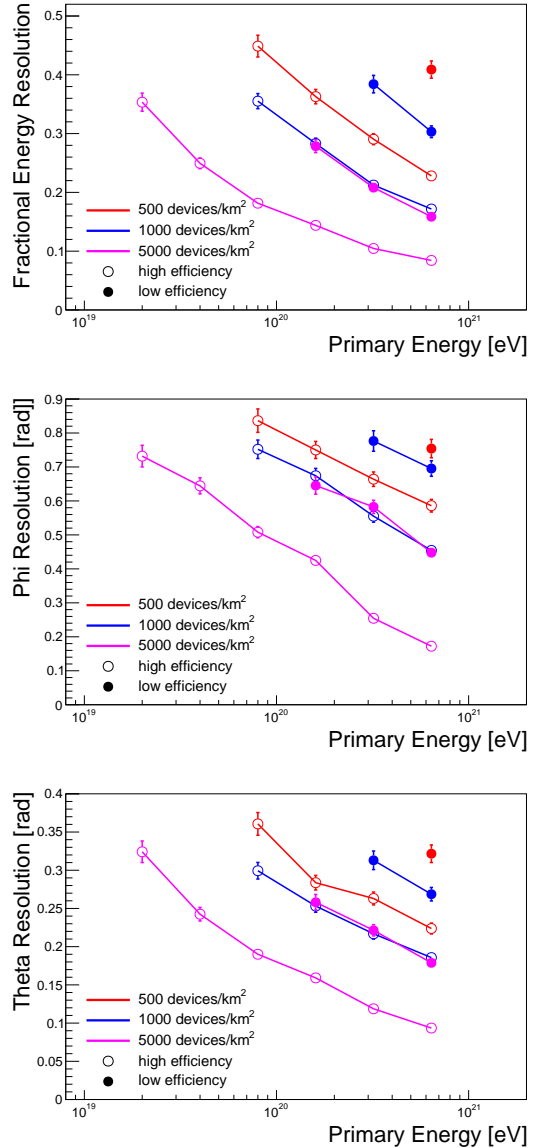


FIG. 6: Fractional energy resolution (top), and ϕ (middle) and θ (bottom) resolution in radians, for simulated events. In the high-efficiency scenario $A\epsilon = 5 \times 10^{-5} \text{ m}^2$ for muons and $5 \times 10^{-9} \text{ m}^2$ for gamma rays. In the low-efficiency scenario $A\epsilon = 1 \times 10^{-5} \text{ m}^2$ for muons and $1 \times 10^{-9} \text{ m}^2$ for gamma rays. Also shown are three different device densities.

where r is the distance of a detector element to the vector of the original incident particle, r_M is the Moliere radius in air, s is the shower age ($s = 1$ being the shower maximum) and N_i is the number of particles of species i in the shower. This parameterization has been validated in realistic simulations from CORSIKA, see Fig 1. This approach neglects some sources of systematic uncertainty, such as the hadronic interaction model, fluctuations of the shower shape, dependence on the atmospheric conditions, and dependence of ρ on the initial particle species. Therefore, the resolutions quoted below should be seen as

an optimistic lower bound; performance of a real network is likely to be significantly worse.

We use an unbinned likelihood to extract incident particle energy and direction:

$$L(N, \theta, \phi) = \prod_i P_0(x_i, y_i) \prod_j P_1(x_j, y_j)$$

where the i index runs across phones that did not reconstruct a candidate and the j index runs across phones that did reconstruct a candidate. The symmetric use of phones with and without candidates naturally handles the non-uniform distribution of participating phones. In areas of high particle density, the possibility exists of multiple hits on a single phone, allowing for additional power in determining the shower density. We leave this for later refinements.

Expected performance in simulated events drawn from Eq. 1 is shown in Fig. 6 for various scenarios in $A\epsilon$ and phone density. The resolution improves with higher shower energy due to higher statistics from an increased particle density. Lower values of $A\epsilon$ can be compensated by higher phone densities, as shown by the overlapping curves.

The background, due to electronic noise, uncorrelated muons and ambient radioactivity, is not expected to be correlated among phones. Assuming the background rate is dominated by cosmic ray muons with flux of $1 \text{ cm}^{-2} \text{ min}^{-1}$, the expected number of uncorrelated background hits during a 100 ms coincidence window in the high-efficiency scenario is $\eta = 0.0008$. Fig. 7 compares the rate of several experimental observables for pure combinatorial background and simulated showers with primary energy $E > 5 \times 10^{19} \text{ eV}$ and $E > 1 \times 10^{20} \text{ eV}$. The rate of high-energy showers is many orders of magnitude lower than the rate at which candidate events are acquired, so extremely rare coincidences can produce a relatively large number of phone hits at rates comparable to high-energy showers. However, the log likelihood ratio (LLR) between the best fit shower and pure combinatorial background is a powerful discriminant. The rate of combinatorial background events depends on the timing resolution of the devices. Similar studies have been performed for larger coincidence windows with qualitatively similar results, though the rate of such background events rises with larger windows.

Expected Observational Power

The per-shower efficiency is calculated in simulation by sampling randomly placed phones in the path of a shower and determining the number of phones which register a hit. To suppress the background from uncorrelated hits, we choose a benchmark requirement that at least five

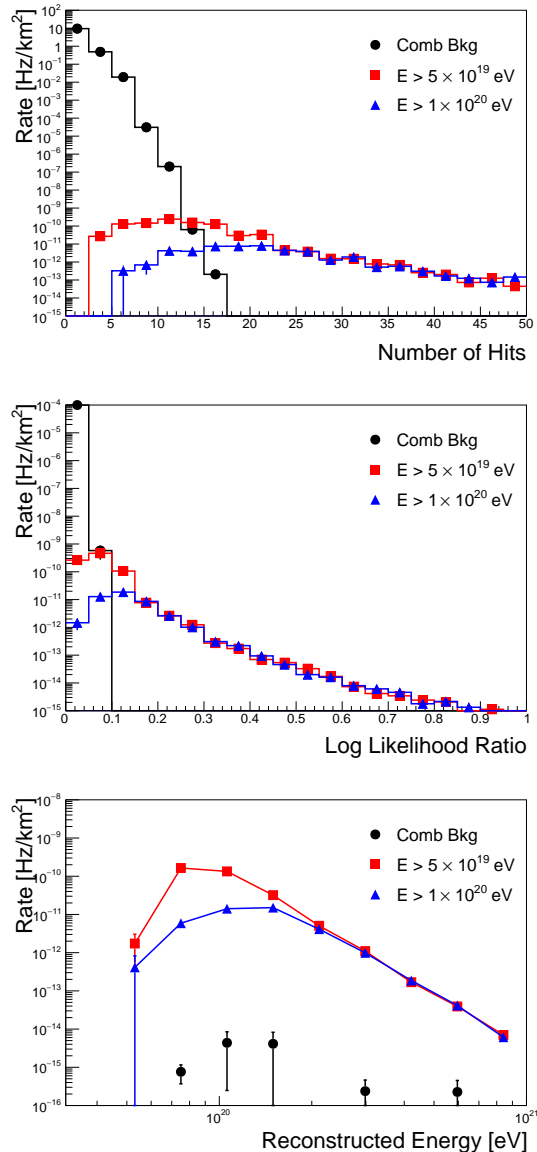


FIG. 7: For a 1 km^2 grid, the expected observation rate of (top) total number of phones registering a hit, (middle) log likelihood ratio of the best fit shower to pure combinatorial background, and (bottom) reconstructed primary energy, for irreducible combinatorial background only, primary showers with energy greater than $5 \times 10^{19} \text{ eV}$, and primary shower with energy greater than $1 \times 10^{20} \text{ eV}$. These plots assume the optimistic muon efficiency benchmark ($A\epsilon = 5 \times 10^{-5} \text{ m}^2$) and a timing resolution of 100 ms.

phones register a hit to be considered a shower candidate; see Fig. 8. The per-shower efficiency is then the fraction of showers which have at least five phones registering hits. The efficiency is a strong function of the density of participating devices, see bottom panel of Fig. 8. In addition, the per-shower efficiency rises with incident particle energy due to the increase in the number of particles in the shower. The dominant contribution at all

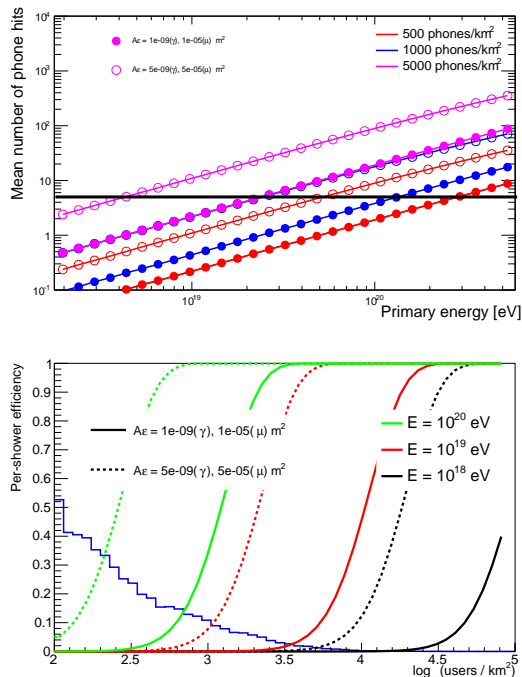


FIG. 8: Top, mean number of phones registering particle hits per shower versus incident primary particle energy, for two choices of per-phone area times efficiency ($A\epsilon$) and three examples of user adoption density. Bottom, per-shower efficiency as a function of the density of users in a 1-km² region; overlaid is the relative distribution of actual population densities [26] with arbitrary normalization.

angles is from muons, due to their much larger efficiency, despite their rarity with respect to photons in vertical showers.

The observing power of state-of-the-art dedicated ground arrays is determined by the *effective area*, which is the integral of the per-shower efficiency over the detector area. We leave considerations of the angular field of view for future studies. For Auger, efficiency for showers above $E = 10^{20}$ eV is effectively 100%, giving an effective area of 3000 km², the size of the instrumented area. To achieve a similar efficiency and effective area would require a density of approximately 400 dedicated devices per km² for the optimistic $A\epsilon$ scenario, distributed over 3000 km², for a total of 1.2M devices.

In practice, we expect the location of devices to be tied to existing population distributions. To assess the size of a network needed to match the effective area of Auger, we perform an analysis similar to Ref. [27] and calculate the effective area of a network composed of the devices of a fraction f of the world population. Population data [26] at the granularity of 30 arc-sec² (0.5-0.8 km² depending on latitude) are overlaid with the efficiency curves in the top pane of Fig 8. In Fig. 9, the effective area for several cases are shown as a function of the fractional user adoption. In the optimistic $A\epsilon$ scenario, less than 1%

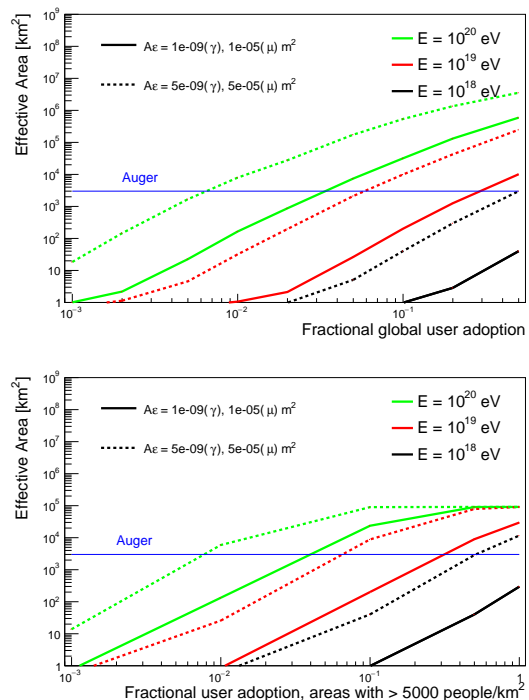


FIG. 9: Top, effective area as a function of the fraction of the global population which participates, for several choices of primary cosmic-ray energy and two choices of per-phone efficiency benchmarks. Bottom, effective area as a function of the fraction of the population in very high density regions (areas with > 5000 people per km²).

user adoption (≈ 45 M users) is needed to match the effective area of Auger for UHECRs.¹ This effective area is dominated by high-density areas due to their higher per-shower efficiency; therefore, the deployment strategy should focus on recruiting contributors in high-density areas. The bottom pane of Fig. 9 shows that the same effective area can be achieved with the same user fraction when restricted to areas with population density greater than 5000/km², which corresponds to ≈ 7 M users. The effective area is only significantly reduced by restricting to these high-density areas when the fractional user adoption is high.

In low population density areas, small clusters of phones can also contribute significantly to the total effective area, though with degraded energy and angular resolution. The per-shower efficiency is a strongly non-linear function of the number and arrangement of phones due

¹ A similar calculation [27] yielded a much smaller estimate of the effective area at $E = 10^{20}$ eV due to an assumption of zero per-shower efficiency for device densities less than 1000/km²; see Ref. [27] for discussion of this assumption. This smaller estimate of the effective area leads to a corresponding larger estimate of the required user fraction.

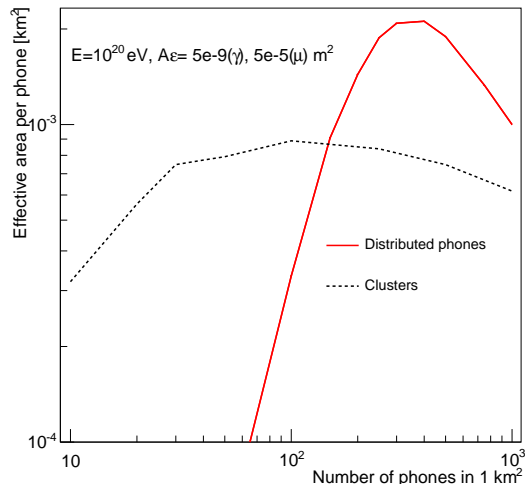


FIG. 10: Effective area per phone for showers with $E = 10^{20}$ eV under the optimistic $A\epsilon$ scenario, as a function of the number of phones in a 1-km^2 square under two clustering possibilities: either the phones are randomly distributed, or grouped in a small cluster. For high densities ($N > 100/\text{km}^2$), distributed phones have the largest contributions. For low densities ($N < 100/\text{km}^2$), clusters can make significant contributions.

to the requirement of a 5-phone coincidence. Figure 10 shows that clusters of 30 or more phones provide an effective area per phone that is within a factor of 2-3 of a uniformly random distribution with 400 phones per km^2 . For example, 134k (15k) localized clusters of 30 (250) phones can also achieve an effective area of 3000 km^2 . Such clusters might be constructed from donated phones no longer in active use, which motivates a deployment strategy that includes partnerships with schools and science clubs around the world.

Note that these calculations assume continuous operation; some degradation of observational power is expected, as some phones may only join the network during night-time charging. On the other hand, users may dedicate devices no longer in active use. The observational power of such a network clearly hinges on the level of user adoption and continued participation.

Conclusions

We propose a novel strategy for observing air showers due to ultra-high energy cosmic rays: an array composed of smartphones running a dedicated app. We have measured the per-phone sensitivity to the particles which comprise the showers and estimated the number of phones needed to achieve observing power to rival the most sensitive current observatories.

Building an installed user base of more than 1M de-

vices operating reliably poses a social and organizational challenge. We have begun to address these by reducing the barriers to participation via unobtrusive operation, and providing incentives for users.

A large network of devices would have unprecedented observing power at energies above 10^{20} eV, where current ground arrays become saturated [28]. Lack of observations of UHECRs above this energy could therefore provide powerful limits on the incident flux.

Such a world-wide network of devices sensitive to muons and photons could also have many other potential uses, such as monitoring local radiation levels. In addition, this global network would be the first of its kind, opening a new observational window to unanticipated processes.

Acknowledgements

We thank Davide Gerbaudo, Tatiana Rodriguez, Josh Cogliati, Rocky Dendo, Steve Barwick, Gourang Yodh, John Beacom, Jonathan Wallick for useful conversations, alpha testing and source calibration.

-
- [1] J. Abraham et al. (Pierre Auger Collaboration), *Astropart.Phys.* **29**, 188 (2008), 0712.2843.
 - [2] J. Abraham et al. (Pierre Auger Collaboration), *Science* **318**, 938 (2007), 0711.2256.
 - [3] A. R. Bell, *Mon.Not.Roy.Astron.Soc.* **182**, 147 (1978).
 - [4] R. Blandford and D. Eichler, *Phys.Rept.* **154**, 1 (1987).
 - [5] E. Waxman, *Phys.Rev.Lett.* **75**, 386 (1995), *astro-ph/9505082*.
 - [6] T. J. Weiler, *Astropart.Phys.* **11**, 303 (1999), *hep-ph/9710431*.
 - [7] R. Abbasi et al. (High Resolution Fly's Eye Collaboration), *Phys.Rev.Lett.* **92**, 151101 (2004), *astro-ph/0208243*.
 - [8] M. Takeda, N. Hayashida, K. Honda, N. Inoue, K. Kadota, et al., *Phys.Rev.Lett.* **81**, 1163 (1998), *astro-ph/9807193*.
 - [9] J. Abraham et al. (Pierre Auger Collaboration), *Phys.Rev.Lett.* **101**, 061101 (2008), 0806.4302.
 - [10] K. Greisen, *Phys.Rev.Lett.* **16**, 748 (1966).
 - [11] G. Zatsepin and V. Kuzmin, *JETP Lett.* **4**, 78 (1966).
 - [12] A. Aab et al. (Telescope Array Collaboration, Pierre Auger Collaboration), *Astrophys.J.* (2014), 1409.3128.
 - [13] T. Abu-Zayyad et al. (Telescope Array), *Astrophys.J.* **768**, L1 (2013), 1205.5067.
 - [14] N. Hayashida et al. (AGASA Collaboration), *Astropart.Phys.* **10**, 303 (1999), *astro-ph/9807045*.
 - [15] URL <http://www.ergotelescope.org/>.
 - [16] J. J. Cogliati, K. W. Derr, and J. Wharton (2014), 1401.0766.
 - [17] A. R. Smith, R. J. McDonald, D. C. Hurley, S. E. Holland, D. E. Groom, W. E. Brown, D. K. Gilmore, R. J. Stover, and M. Wei, in *Sensors and Camera Systems for Scientific, Industrial, and Digital Photography Applica-*

- tions III*, edited by M. M. Blouke, J. Canosa, and N. Sampat (2002), vol. 4669 of *Society of Photo-Optical Instrumentation Engineers (SPIE) Conference Series*, pp. 172–183.
- [18] DECO, APS News **21**, 3 (2012).
- [19] URL <http://crayfis.io/>.
- [20] D. Heck, G. Schatz, T. Thouw, J. Knapp, and J. Capdevielle (1998).
- [21] S. Ostapchenko, Phys.Rev. **D83**, 014018 (2011), 1010.1869.
- [22] H. S. Matis, F. Bieser, G. Rai, F. Retiere, H. G. Ritter, et al., IEEE Trans.Nucl.Sci. **50**, 1020 (2003), nucl-ex/0212019.
- [23] S. Kleinfelder, S.-K. Lim, X. Lui, and A. El Gamal, IEEE Journal of Solid-State Circuits **36** (2001).
- [24] S. Agostinelli et al. (GEANT4), Nucl.Instrum.Meth. **A506**, 250 (2003).
- [25] P. Grieder, *Extensive Air Showers* (Springer, 2010).
- [26] URL <http://sedac.ciesin.columbia.edu/data/set/grump-v1-population-density>.
- [27] M. Unger and G. Farrar (2015), 1505.04777.
- [28] A. Aab et al. (Pierre Auger Collaboration) (2013), 1307.5059.